

Extraction Of Fractional Inspiratory Time And Respiration Rate From Electrocardiogram Signals

Maria Nyamukuru, Kofi Odame

Thayer School of Engineering, Dartmouth College
14 Engineering Drive
Hanover, NH 03755

maria.t.nyamukuru.th@dartmouth.edu, kofi.odame@dartmouth.edu

Abstract

At-home monitoring of lung health enables the early detection and treatment of respiratory diseases like asthma and chronic obstructive pulmonary disease (COPD). To allow for discreet continuous monitoring, various approaches have been proposed to estimate the respiratory rate from an electrocardiogram (ECG) signal. Unfortunately, respiratory rate can only provide a non-specific, incomplete picture of lung health. This paper introduces an algorithm to extract more respiratory information from the ECG signal: in addition to respiratory rate, the algorithm also derives the fractional inspiratory time (FIT), which is a direct measure of airway obstruction. The algorithm is based on a gated recurrent neural network that infers vital respiratory information from a two-lead ECG signal. The network is trained and tested on different test subjects and reports up to 0.099, and 0.243 normalized root mean squared error in the computation of FIT and respiration rate, respectively.

Keywords: electrocardiogram (ECG), bio-signals, respiration, inspiration-expiration (I:E) ratio, T_i/T_{tot} , fractional inspiratory time (FIT), lung performance, neural network, gated recurrent unit, ECG-derived respiration (EDR)

1 Introduction

There are 251 million people worldwide who suffer from chronic obstructive pulmonary disease (COPD), and risk experiencing a sudden flare up in their symptoms. Early detection and treatment of COPD exacerbations would increase patients' quality of life, reduce mortality, and avoid the majority of COPD-related healthcare costs.

One of the most predictive signs of an impending COPD exacerbation is an increase in lung airway obstruction, measured via spirometry. But there is no way to perform spirometry reliably at home, due to low patient adherence and poor patient technique.

An alternative to home spirometry is to monitor lung health via an electrocardiogram-derived respiratory (EDR) signal: it requires no special patient technique, and it is integrable into a smartwatch, thus encouraging patient adherence. Unfortunately, EDR is of limited use because it primarily measures respiratory rate (Charlton et al. 2018), which provides an incomplete, non-specific picture of lung health.

US Patent Application No.: 63/120,085. All rights reserved.

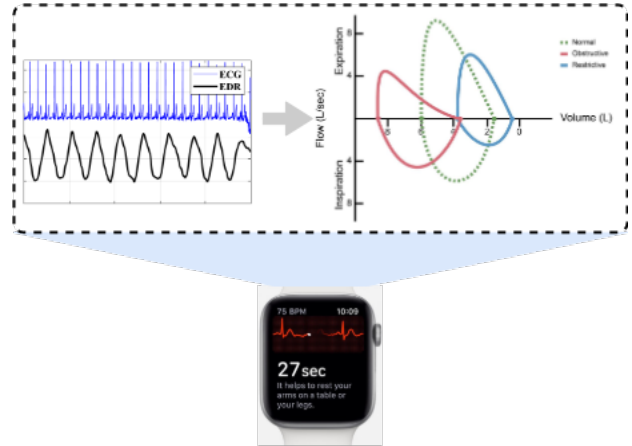


Figure 1: Continuous lung function monitoring from ECG signals (Dominguez 2020),(Apple 2020)

To address the limitations of EDR, this paper introduces an algorithm to extract more respiratory information from the electrocardiogram signal: in addition to respiratory rate, the algorithm also derives the fractional inspiratory time (FIT), which is a direct measure of airway obstruction. In this paper, we will discuss how to extract FIT from ECG signals successfully.

2 Respiratory Signal Modulation of ECG

Breathing affects the ECG signal in three main ways: ECG frequency modulation, ECG amplitude modulation, and ECG baseline wander, all of which can be used to extract the respiratory signal.

ECG frequency modulation, also known as Respiratory Sinus Arrhythmia (RSA), refers to the heart rate variability associated with respiration (Caiani et al. 1999). During inspiration, the heart rate increases because the diaphragm contracts downwards creating a negative pressure in the thoracic cavity which increases the pull of blood into the heart's veins and increases the amount of blood in the heart. On the other hand, expiration causes a drop in heart rate due to less negative pressure in the thoracic cavity, so less blood is pulled into the heart. These variations in heart rate with breathing cycle are observed as changes in the interval be-

tween adjacent R peaks of the ECG (of the European Society of Cardiology the North American Society of Pacing Electrophysiology 1996).

ECG amplitude modulation results from the change in the electric heart vector with reference to the electrodes due to rise and fall motion of the lungs during breathing (Travaglini et al. 1998). During inspiration, the diaphragm contracts and shifts downwards, and during expiration, the diaphragm expands and shifts upwards. The movement of the diaphragm changes the positioning of the heart, by moving it towards the abdomen when it expands and towards the chest when it contracts. This adjustment in the heart causes changes in the electric heart vector and in turn modulates the ECG signal, particularly the QRS complexes (Arunachalam and Brown 2009) which can be demodulated to extract the respiratory signal as shown in Fig. 3.

Less commonly, the respiratory signal is extracted from the ECG signal’s baseline wander. The expansion and contraction of the chest causes the electrodes placed on the chest to move closer and further away from the heart, resulting in the low frequency component of the ECG signal, also known as the baseline wander (Ji et al. 2008). ECG frequency modulation, ECG amplitude modulation, and baseline wander excel in extracting the respiration signal’s frequency component, making them ideal in determining the respiratory rate. They, however, fall short in accurately extracting the phase information of the respiratory signal.

3 Related Work

In order to extract both frequency and phase information, different techniques have been proposed like principal component analysis (PCA) (Langley, Bowers, and Murray 2010), and kernel principal component analysis (kPCA) (Widjaja et al. 2012). These techniques require use of handcrafted features like P-peak, Q-peak, R-peak, S-peak and T-peak amplitudes, and RR-interval (Gao et al. 2017), to extract a more accurate EDR signal. Another technique to extract the respiratory signal from ECG utilizes Hilbert transformations to break down the ECG into different sinusoids. This technique then utilizes Hilbert vibration decomposition to filter the sinusoids whose amplitudes are of a lower order (Sharma and Sharma 2018). Using the Hilbert transform negates the use of handcrafted features but only utilizes a small portion of the ECG signal to extract the respiratory signal.

In order to extract both the frequency and phase information of the respiratory signal with high accuracy and without using handcrafted features while using majority of the ECG signal, we propose a novel approach to perform an end-to-end extraction of respiratory signals from ECG signals using a gated recurrent unit neural network. To accurately extract respiratory frequency information, we focus on the respiratory rate, and focus on the FIT to accurately extract phase information. We formulate the problem to maximize the accuracy of predicting the respiratory rate and FIT of the respiratory signal as discussed in Section IV.

4 Theory

The computation of the FIT and respiratory rate is dependent on correctly identifying the inspiratory phase and expiratory phase of the respiration signal, as shown in Fig. 2b. This reconstruction relies on accurately locating the peaks and valleys, as shown in Fig. 2a.

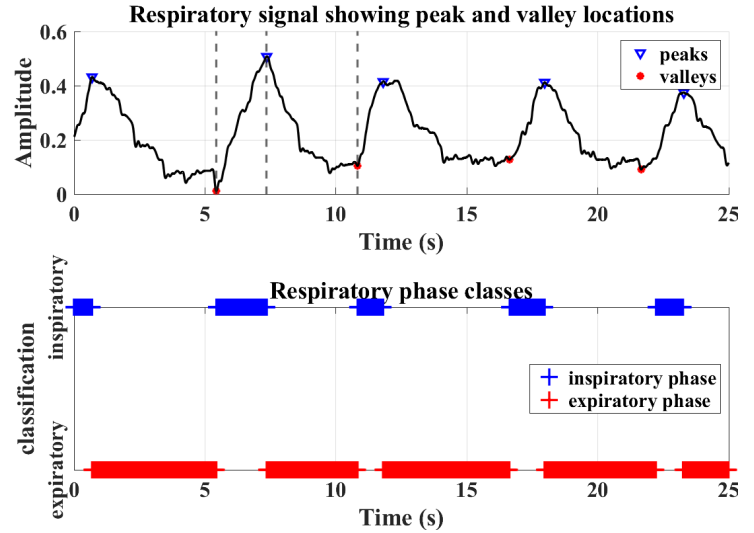


Figure 2: a. Respiratory signal (top), b. Inspiratory and Expiratory Phase Classification (bottom)

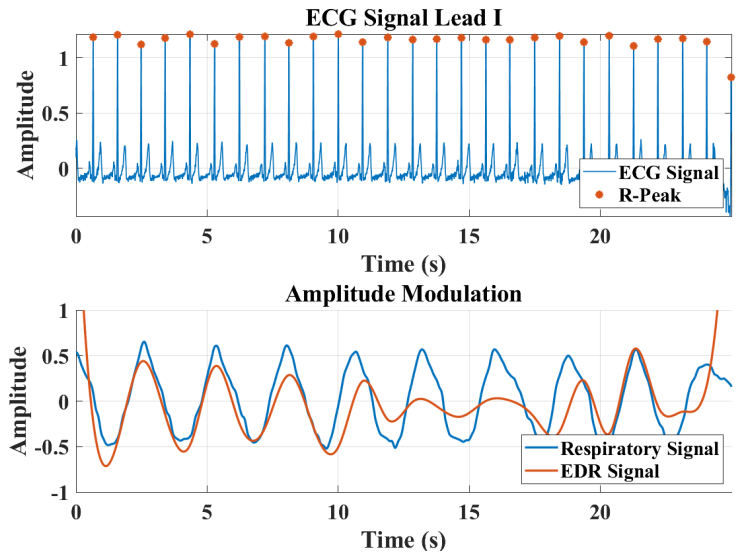


Figure 3: a. R-Peak Detection on ECG Lead I Signal (top), b. EDR vs Respiratory signal (bottom)

One approach is to reconstruct the respiratory signal from the ECG signal as discussed in Sections 2 and 3. For example, Fig. 3 shows the reconstructed respiratory signal based on amplitude modulation and spline interpolation. This EDR signal is used to deduce the inspiratory peaks and expiratory valleys.

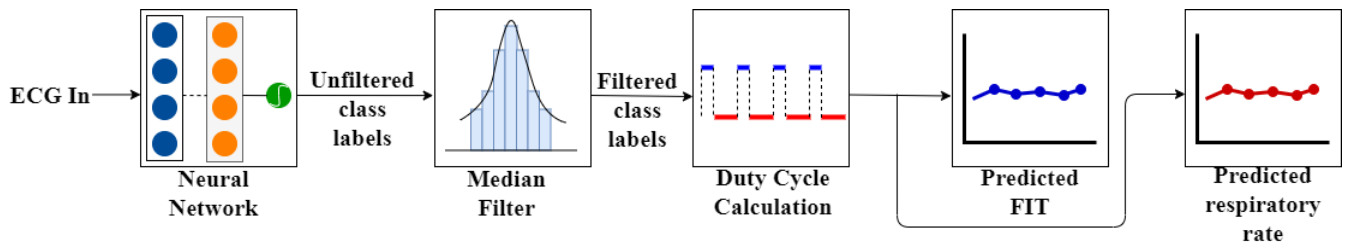


Figure 4: Block diagram showing novel approach to extract FIT and respiratory rate from ECG signals using GRU network to classify underlying inspiratory and expiratory phases, a median filter to filter the noisy classification output and a duty cycle calculation to compute FIT and respiratory rate

To avoid the use of spline interpolation, or any hand-crafted features, and to utilize the entire ECG signal data, respiratory signal reconstruction could be set up as a regression problem. This requires the use of temporally aligned ECG signal data and respiratory signal data to train on. The regression model would output a respiration signal, and a peak/valley detection algorithm would then be applied to further locate the inspiratory peaks and expiratory valleys. This approach, however, requires two algorithms to extract the FIT: the regression algorithm and the peak/valley algorithm, making it susceptible to compounding errors.

In an effort to combine these two algorithms and circumvent their drawbacks, we formulate the problem as a two-class classification problem; the two classes are the inspiratory phase and the expiratory phase. The inspiratory peak and the expiratory valley mark the transition from inspiration-expiration and expiration-inspiration, respectively, as shown in Fig. 2b. This formulation simplifies the learning task and emphasizes the importance of correctly identifying peaks and valleys, which is essential in calculating FIT and determining the respiratory rate. Additionally, since the peak/valley detection is integrated into the classification formulation, a separate peak/valley algorithm is not required. This approach consists of three main stages, as shown in Fig. 4; the neural network stage that performs classification of inspiratory and expiratory phases from input ECG signals, the median filter that removes any noise in the classified output, and the duty cycle calculation that computes the FIT and the respiratory rate.

The neural network stage is the most crucial stage of this approach, making the choice of neural network architecture essential. The gated recurrent unit (GRU) (Cho et al. 2014) is explored to solve the two-class classification problem. The GRU is a variant of the recurrent neural network (RNN), a neural network design that models time dependencies. The GRU’s variation contains reset and update gates, which provide inbuilt memory to better capture long-term temporal dependencies for large time steps without experiencing vanishing gradients during back-propagation. This GRU trait is responsible for its excellent performance on sequence-to-sequence labeling tasks, like speech recognition, music modeling, and natural language processing. GRU networks are also more robust to noisy sequential data. A similar RNN variant to the GRU is the LSTM. The LSTM has an additional gate, the forget gate. The LSTM is not used in this

problem because it has significantly more parameters than the GRU, and the GRU has better performance for smaller and less frequent datasets (Chung et al. 2014), making it ideal for this application. These GRU characteristics make it ideal for the extraction and classification of inspiratory and expiratory phases from ECG signals.

5 Materials and methods

5.1 Dataset

The Fantasia database (Iyengar et al. 1996) is a common test set for evaluating EDR algorithms. However, it does not have temporally aligned ECG and respiratory signals (Nyamukuru and Mark 2020) and is therefore unsuitable for our application. The data used in this study is from the Combined measurement of ECG, Breathing, and Seismocardiograms (CEBS) database (García-González et al. 2013), which is publicly available on PhysioNet (Goldberger et al. 2000). This database contains recordings of the respiratory signal, ECG Lead I signal, ECG Lead II signal, and Seismocardiograms (SCG) signal. The ECG Lead I, ECG Lead II, and the respiratory signals are the signals of interest. These signals were collected simultaneously and are, therefore, temporally aligned. (García-González et al. 2013) details how this data was acquired.

We reviewed the data available and selected the measurements of six subjects whose respiratory signal profiles were closest to a typical respiratory signal profile. This selection formed a six-hour total dataset used for training and testing the neural network.

5.2 Preprocessing

During preprocessing, the dataset is down-sampled from 5000 Hz to 300 Hz to reduce power consumption and memory usage. 300 Hz is chosen as the new sampling frequency because it is the lowest sampling frequency that can be used to satisfy the Nyquist sampling theorem, given that the maximum bandwidth is 150 Hz at the ECG signal channels. A third-order median filter is then applied to the respiratory signal to attenuate the noise. All the input signals, that is to say, the ECG Lead I, ECG Lead II, and the respiratory signals are normalized in the 0 to 1 range. Each normalized ECG Lead signal is used as one of the features in the two-dimensional input signal, x , to the neural network.

Each sample point in the respiratory signal time series is labeled using the following semi-automatic procedure. First, the peaks and troughs of the respiratory signal are labeled manually. Then, all points between a given trough and the next peak in the time series are automatically labeled class 1 (inspiratory phase). All points between a given peak and the subsequent trough are labeled class 0 (expiratory phase) as shown in Fig. 2b. The resulting time series of class labels, y , are used as the target output to train the neural network.

For neural network training, both input signal, x , and class labels, y , are partitioned into 25 second windows of 7500 samples.

5.3 Model Design

The GRU network consists of three 16-unit hidden GRU layers, one 16-unit fully connected layer, and a single unit output layer, as shown in Fig. 5. The network processes 25-second long (7500 samples) sequences and returns output for each sample in the sequence. The GRUs' ability to capture long-term dependencies makes them ideal for extracting temporal and spatial features from the 2-feature ECG input signals.

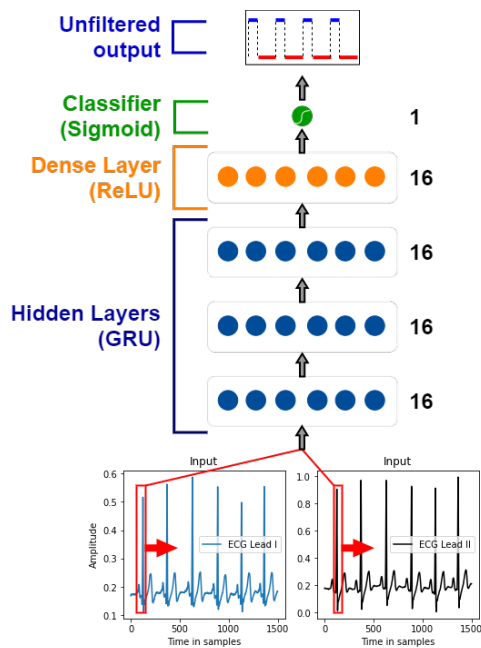


Figure 5: GRU network architecture that takes in 2 features at a time (one sample), the ECG Lead I and Lead II, and outputs respiratory phase classes for each sample for a 25-second window (7500 samples), with no overlap

The hidden layers feed into a fully connected layer/ dense layer that consists of 16 rectified linear units (ReLU). The fully connected layer feeds into the classification layer with a sigmoid function that outputs each sample's class label in the sequence.

5.4 Postprocessing

The noise from the input ECG signal that propagates through the neural network is mitigated by applying a 33^{rd} order median filter to every predicted output window. This noise filtering removes spurious inspiratory and expiratory phases of less than 100 ms, thereby improving the predicted output accuracy. The median filtered output is used to compute FIT.

5.5 FIT Extraction

Before calculating the FIT, the algorithm identifies the number of complete cycles N_c . A complete cycle includes an inspiratory phase and an expiratory phase. The algorithm computes the FIT for each complete respiration cycle as shown in Equation 1 where N_i is the number of samples in the inspiratory phase and N_{tot} is the total number of samples in the complete cycle, which is the sum of samples in the inspiratory and expiratory phases.

$$FIT = \frac{N_i}{N_{tot}} \quad (1)$$

5.6 Respiratory rate Extraction

The respiratory rate is computed for each 25-second window as shown in Equation 2 where F_s is the sampling frequency, N_c is the total number of complete cycles in each window by and S_{tot} is the total number of samples in the complete cycles.

$$\text{respiratory rate} = F_s \cdot 60 \cdot \frac{N_c}{S_{tot}} \quad (2)$$

6 Experiments

The neural network shown in Fig. 5 is designed and implemented using Tensorflow Keras v2.2 (Chollet et al. 2015). The hyper-parameters of the network were initially determined using hyperas (Pumperla 2020), a hyper-parameter optimization library, and then tweaked manually to reduce the number of parameters whilst achieving similar performance. The hyper-parameters used to train this network are as shown in Table 1.

Table 1: Neural Network Hyper-parameters

Parameter	Value
Epochs Used	500
Batch Size	32
Training Optimizer	Adam (Kingma and Ba 2015)
Learning rate	0.005
Number of parameters	4530

During training, a 20% cross-validation training split allows the model to train on multiple train-validation splits. In order to guarantee that the algorithm uses the best performing model, a model checkpoint is implemented to save and retrieve the model with the highest validation accuracy. However, since the expiratory phase of a normal person lasts longer than the inspiratory phase, the expiratory phase will have a higher representation in the dataset making the algorithm biased towards the expiratory phases. To address this

bias, we used sample weights to normalize the binary cross-entropy loss function. The application of sample weights to the loss function results in an evenly distributed prediction accuracy for both the inspiratory phases and the expiratory phases. The neural network training and testing occur in two stages.

6.1 Base Model

Initially, the neural network is trained on five of the six subjects and evaluated on the test subject whose data is not included in the training set. This is done for all combinations of the six subjects, I, II, III, IV, V and VI, resulting in six base models one for each test subject. This case informs how well the network works without seeing data from the test subject. The base model weights are used to fine-tune the neural network model with new training data.

6.2 Fine-tuned Model

The second stage consists of fine-tuning the base model on data from the test subject that was initially excluded from the training set. The model is fine-tuned on 5-minute incremental amounts of data from 5 minutes up to 20 minutes. Forty minutes of data from the test subject is reserved for evaluating both the base model and the fine-tuned models.

7 Results

The trained base models and fine-tuned models are evaluated on the same test sets. An exemplary plot of the accuracy and loss curves during the training and validation of the base model on Subject VI is shown in Fig. 6.

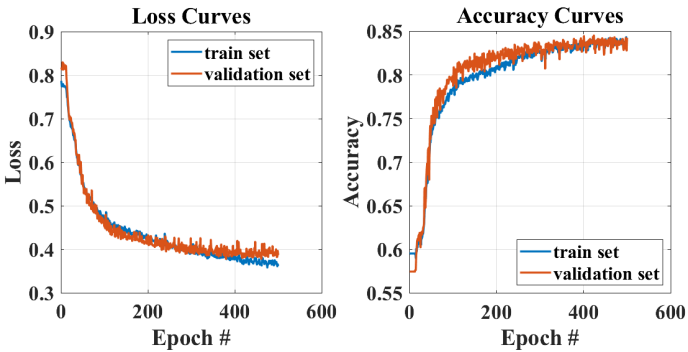


Figure 6: Accuracy and Loss Training Curves for Subject VI

The median filter filters the noise in the neural network outputs, and the test accuracy, precision, recall, and F1-score of the filtered output are recorded. Table 2 below shows the results for Subject VI for all neural network models, base and fine-tuned models with different amounts of data.

The test accuracy results from all subjects for all models are shown in Fig. 7.

The FIT is computed for every complete cycle in each 25-second window of the filtered predicted classes output test sets, and is compared to the FIT from the true classes as shown by the exemplary plots in Fig. 10 for Subject III - 10 minutes and Fig. 11 for Subject V - 15 minutes. The average

Table 2: Evaluation of base and fine-tuned GRU models

	Subject VI Evaluation Results in %			
	Test Acc.	F1-Score	Precision	Recall
0 mins*	42	42	45	45
5 mins	89	89	90	89
10 mins	90	90	90	90
15 mins	91	91	91	91
20 mins	91	91	91	91

* Base model

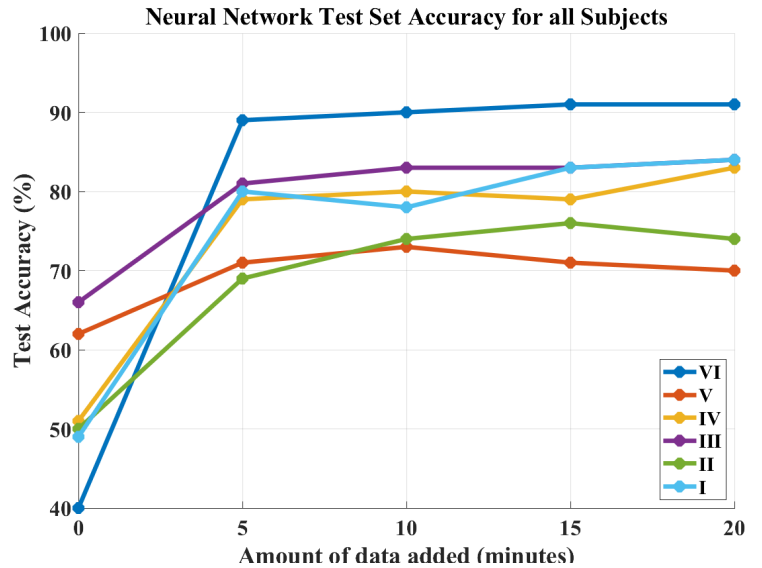


Figure 7: Filtered classification output test set accuracy of all subjects

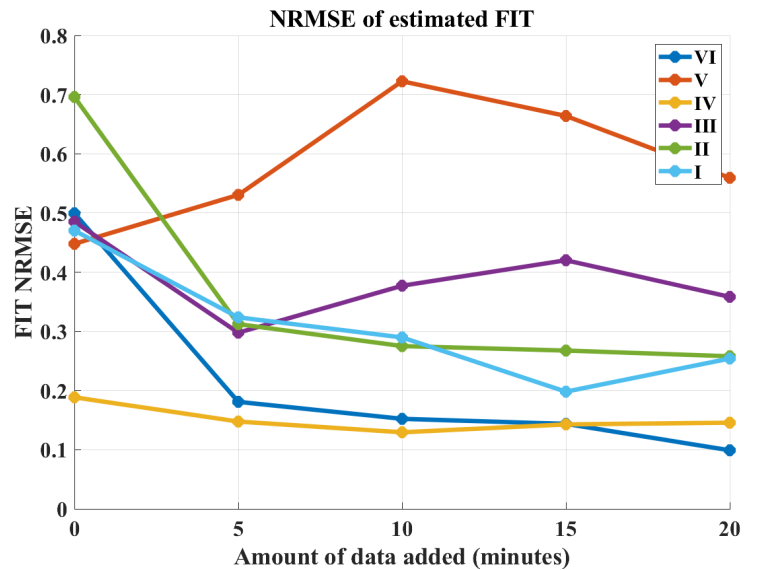


Figure 8: NRMSE of the FIT for all subjects

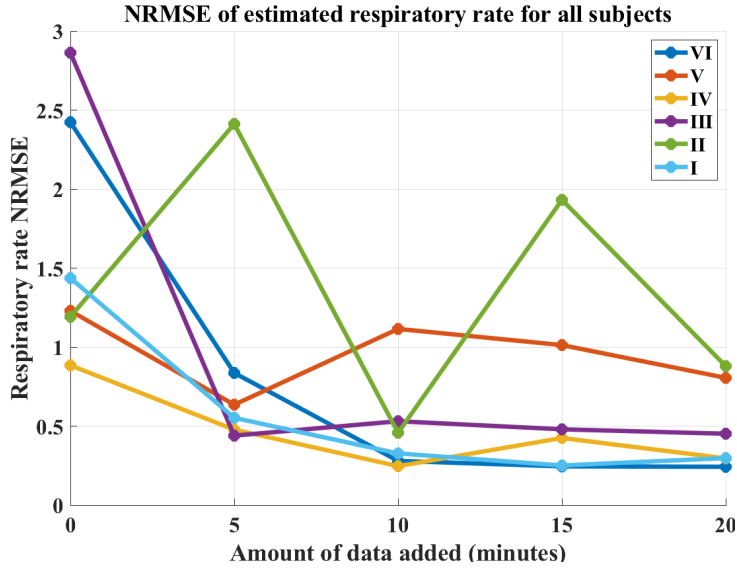


Figure 9: NRMSE of the respiratory rate for all subjects

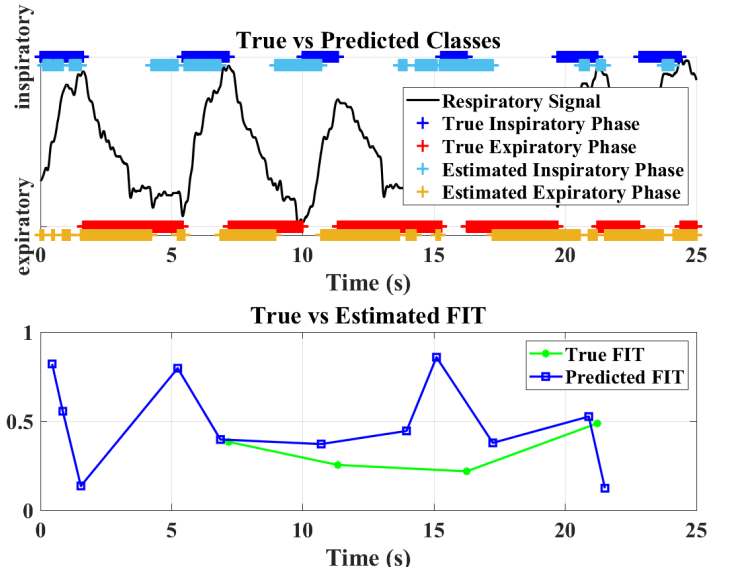


Figure 11: a. Plot of true vs predicted classes output of one window for Subject V (top) and b. Plot of true vs predicted FIT of one window for Subject V (bottom)

FIT for each 25-second window in the test set is computed and used to calculate the normalized root mean squared error (NRMSE) of estimated FIT and respiratory rate obtained from this novel approach, as shown in Fig.8 and Fig. 9.

The NRMSE is computed as shown in Equation 3 where \hat{y}_i is the estimated average FIT or respiratory rate for one window, y_i is the true average FIT or respiratory rate for one window, and n is the total number of windows in the test set.

$$\text{NRMSE} = \frac{\sqrt{\sum_{i=1}^n \frac{(y_i - \hat{y}_i)^2}{n}}}{\sum_{i=1}^n \frac{y_i}{n}} \quad (3)$$

Additionally, Bland-Altman plots for the estimated FIT and respiratory rate for all subjects are computed. These plots are used to determine how well the predictions from this approach compare to the ground truth and determine if this technique is interchangeable with the ground truth technique. Two exemplary plots are shown in Fig. 12 and Fig. 13 for Subjects V and VI.

8 Discussion

The lowest classification accuracy and the highest NRMSE for both the FIT and respiratory rate are observed for the base models when data from the test set subject is not included in the training (0 minutes) as shown in Fig. 7, Fig. 8 and Fig. 9. This low performance is attributed to the small dataset which does not allow for a diverse representation of respiratory signals in the training set. This poor performance of the base model is particularly worse for Subject VI who has the lowest accuracy of the base model performance at 40% as shown in Fig. 7. Subject VI has an inspiratory phase that is on average longer than the expiratory phase, and therefore an FIT that is on average above 0.5 as shown in Fig. 10. This is unlike most of the other subjects whose

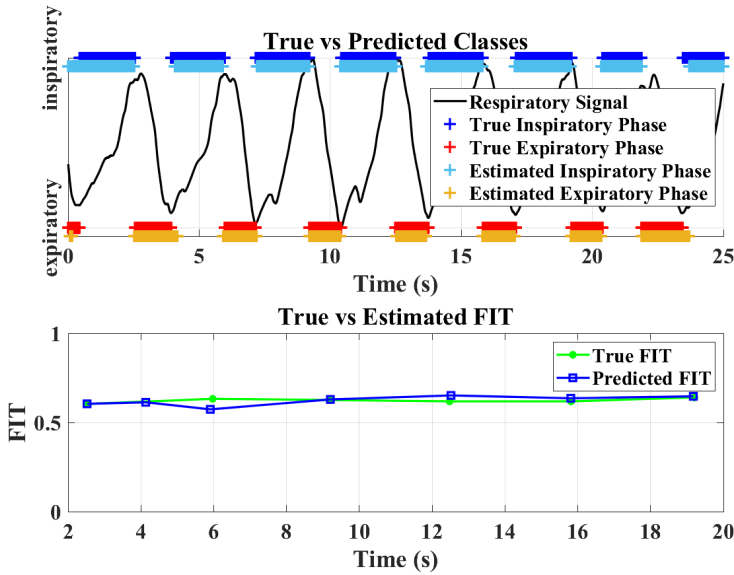


Figure 10: a. Plot of true vs predicted classes output of one window for Subject VI (top) and b. Plot of true vs predicted FIT of one window for Subject VI (bottom)

true average FIT is less 0.5, for example Subject V shown in top plot of Fig. 11. Therefore for the base model, where Subject VI is excluded from the training set and used solely as the test set, the neural network model performs poorly. This is rectified by fine-tuning the neural network model on example data used in the test set.

Fine-tuning the model on example data of the test set results in up to 50% higher classification accuracy, and reduces the FIT NRMSE by up to 0.4 and the respiratory rate NRMSE by up to 2.6. This results in a minimum FIT NRMSE of 0.0990 reported on Subject VI with 20 minutes of fine-tuning data as shown in Fig. 8, and a minimum respiratory rate NRMSE of 0.2428 also reported on Subject VI with 20 minutes of fine-tuning data as shown in Fig. 9. The increase in classification accuracy and the decrease in FIT and respiratory rate NRMSE when fine-tuned on the data from the test subject is attributed to the increase in data's diversity, which allows the model to generalize better. From Figs. 7, 8, 9, increasing the amount of data in the fine-tuned training data generally improves accuracy and reduces the FIT NRMSE and respiratory rate NRMSE. The gain in performance starts to plateau at 10 minutes, and implies that a minimum of 10 minutes should be collected to fine-tune the model for optimal performance.

This improved performance is very evident in the Bland-Altman plots for different subjects. The FIT and respiratory rate Bland Altman plots of the base models for all the subjects have negative proportional bias. This negative proportional bias diminishes, and tends towards a fixed bias with increased data in the fine-tuned models as shown in Fig. 12 and Fig. 13.

The noise seen in the predicted classifications in Fig. 11(b) is due to noisy input signals as shown in Fig. 11(a). These noisy signals are included in the training set and affect the accuracy of the detected FIT. Fig. 10(a) has much cleaner data than Fig. 11(a), and also reports a much more accurate FIT estimation as shown in Fig. 10(b). This proves that the algorithm performs exceptionally well, and has higher test set accuracy and lower FIT and respiratory rate NRMSE for subjects whose fine-tuned training data is cleaner with less false peaks and valleys.

9 Conclusion

This paper proposes a GRU neural network architecture to extract FIT and respiratory rate from an ECG signal. The GRU neural network is demonstrated to have significantly high classification accuracy and, as a resultant accurate FIT and respiratory rate estimation when fine-tuned on at least 10 minutes of clean subject data. This method will allow for implementing this GRU architecture on wearable devices that collect ECG signal data. This technique would increase ECG signals' utility and motivate continuous monitoring of pulmonary parameters from prevalent wrist-worn wearable devices with built-in ECG sensors.

References

Apple. 2020. Apple Watch Series 5. URL <https://www.apple.com/apple-watch-series-5/health/>.

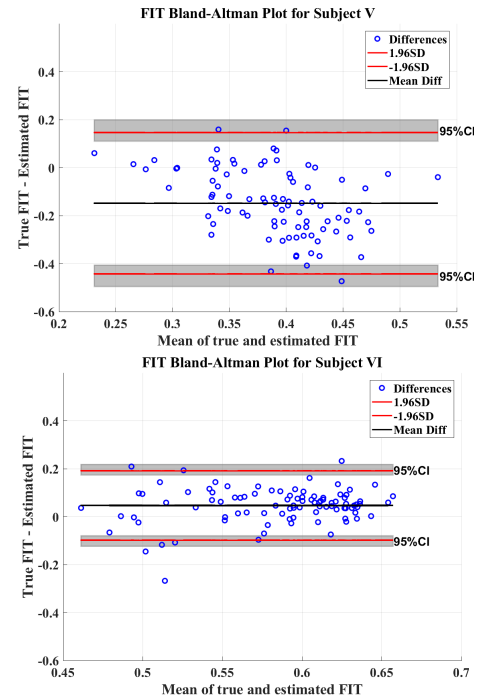


Figure 12: a. Bland-Altman plot of true vs predicted FIT outputs from Subject V-15 minutes (top) and b. Bland-Altman plot of true vs predicted FIT outputs from Subject VI-15 minutes (bottom)

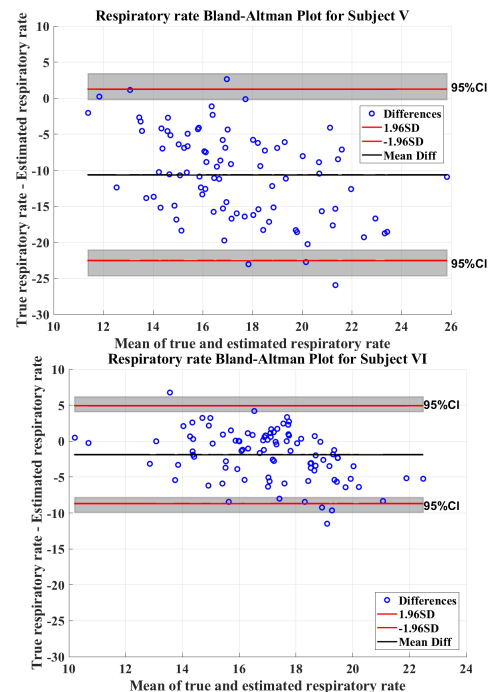


Figure 13: a. Bland-Altman plots of true vs predicted respiratory rate outputs from Subject V-15 minutes (top) and b. Bland-Altman plots of true vs predicted respiratory rate outputs from Subject VI-15 minutes (bottom)

- Arunachalam, S. P.; and Brown, L. F. 2009. Real-time estimation of the ECG-derived respiration (EDR) signal using a new algorithm for baseline wander noise removal. In *2009 Annual International Conference of the IEEE Engineering in Medicine and Biology Society*, 5681–5684.
- Caiani, E. G.; Porta, A.; Terrani, M.; Guzzetti, S.; Malliani, A.; and Cerutti, S. 1999. Minimal adaptive notch filter for respiratory frequency tracking. In *Computers in Cardiology 1999. Vol.26 (Cat. No.99CH37004)*, 511–514.
- Charlton, P. H.; Birrenkott, D. A.; Bonnici, T.; Pimentel, M. A. F.; Johnson, A. E. W.; Alastruey, J.; Tarassenko, L.; Watkinson, P. J.; Beale, R.; and Clifton, D. A. 2018. Breathing Rate Estimation From the Electrocardiogram and Photoplethysmogram: A Review. *IEEE Reviews in Biomedical Engineering* 11: 2–20.
- Cho, K.; van Merriënboer, B.; Gulcehre, C.; Bougares, F.; Schwenk, H.; and Bengio, Y. 2014. Learning phrase representations using RNN encoder-decoder for statistical machine translation. In *Conference on Empirical Methods in Natural Language Processing (EMNLP 2014)*.
- Chollet, F.; et al. 2015. Keras. <https://keras.io>.
- Chung, J.; Gulcehre, C.; Cho, K.; and Bengio, Y. 2014. Empirical evaluation of gated recurrent neural networks on sequence modeling. In *NIPS 2014 Workshop on Deep Learning, December 2014*.
- Dominguez, M. 2020. Pressure-Volume Curve - Respiratory - Medbullets Step 1. URL <https://step1.medbullets.com/respiratory/117003/pressure-volume-curve>.
- Gao, Y.; Yan, H.; Xu, Z.; Xiao, M.; and Song, J. 2017. A principal component analysis based data fusion method for ECG-derived respiration from single-lead ECG. *Australasian Physical & Engineering Sciences in Medicine* 41: 59–67.
- García-González, M. A.; Argelagós-Palau, A.; Fernández-Chimeno, M.; and Ramos-Castro, J. 2013. A comparison of heartbeat detectors for the seismocardiogram. In *Computing in Cardiology 2013*, 461–464.
- Goldberger, A. L.; Amaral, L. A. N.; Glass, L.; Hausdorff, J. M.; Ivanov, P. C.; Mark, R. G.; Mietus, J. E.; Moody, G. B.; Peng, C.-K.; and Stanley, H. E. 2000. PhysioBank, PhysioToolkit, and PhysioNet. *Circulation* 101(23): e215–e220. doi:10.1161/01.CIR.101.23.e215. URL <https://www.ahajournals.org/doi/abs/10.1161/01.CIR.101.23.e215>.
- Iyengar, N.; Peng, C. K.; Morin, R.; Goldberger, A. L.; and Lipsitz, L. A. 1996. Age-related alterations in the fractal scaling of cardiac interbeat interval dynamics. *American Journal of Physiology-Regulatory, Integrative and Comparative Physiology* 271(4): R1078–R1084. doi:10.1152/ajpregu.1996.271.4.R1078. URL <https://doi.org/10.1152/ajpregu.1996.271.4.R1078>. PMID: 8898003.
- Ji, T. Y.; Lu, Z.; Wu, Q. H.; and Ji, Z. 2008. Baseline normalisation of ECG signals using empirical mode decomposition and mathematical morphology. *Electronics Letters* 44(2): 1–2. URL <https://search.proquest.com/docview/1625484001?accountid=10422>.
- Kingma, D. P.; and Ba, J. 2015. Adam: A Method for Stochastic Optimization. *CoRR* abs/1412.6980.
- Langley, P.; Bowers, E. J.; and Murray, A. 2010. Principal Component Analysis as a Tool for Analyzing Beat-to-Beat Changes in ECG Features: Application to ECG-Derived Respiration. *IEEE Transactions on Biomedical Engineering* 57(4): 821–829.
- Nyamukuru, M.; and Mark, R. 2020. Personal correspondence with Mr. Roger Mark, the database administrator on July, 15th 2020.
- of the European Society of Cardiology the North American Society of Pacing Electrophysiology, T. F. 1996. Heart Rate Variability. *Circulation* 93(5): 1043–1065. doi:10.1161/01.CIR.93.5.1043. URL <https://www.ahajournals.org/doi/abs/10.1161/01.CIR.93.5.1043>.
- Pumperla, M. 2020. URL <https://github.com/maxpumperla/hyperas>.
- Sharma, H.; and Sharma, K. K. 2018. ECG-derived respiration based on iterated Hilbert transform and Hilbert vibration decomposition. *Australasian Physical & Engineering Sciences in Medicine* 41: 429–443.
- Travaglini, A.; Lamberti, C.; DeBie, J.; and Ferri, M. 1998. Respiratory signal derived from eight-lead ECG. In *Computers in Cardiology 1998. Vol. 25 (Cat. No.98CH36292)*, 65–68.
- Widjaja, D.; Varon, C.; Dorado, A.; Suykens, J. A. K.; and Van Huffel, S. 2012. Application of Kernel Principal Component Analysis for Single-Lead-ECG-Derived Respiration. *IEEE Transactions on Biomedical Engineering* 59(4): 1169–1176.